DOI: 10.1002/cmdc.201000013

Radiofluorinated Pyrimidine-2,4,6-triones as Molecular Probes for Noninvasive MMP-Targeted Imaging

Hans-Jörg Breyholz,*[a] Stefan Wagner,[a] Andreas Faust,[a] Burkhard Riemann,[a] Carsten Höltke,[b] Sven Hermann,[c] Otmar Schober,[a] Michael Schäfers,[c, d] and Klaus Kopka[a, d]

Matrix metalloproteinases (MMPs) are zinc- and calcium-dependent endopeptidases. Representing a subfamily of the metzincin superfamily, MMPs are involved in the proteolytic degradation of components of the extracellular matrix. Unregulated MMP expression, MMP dysregulation and locally increased MMP activity are common features of various diseases, such as cancer, atherosclerosis, stroke, arthritis, and others. Therefore, activated MMPs are suitable biological targets for the specific visualization of such pathologies, in particular by using radiolabeled MMP inhibitors (MMPIs). The aim of this work was to develop a radiofluorinated molecular probe for noninvasive in vivo imaging for the detection of up-regulated levels of activated MMPs in the living organism. Fluorinated MMPIs (**26**, **31** and **38**) based on the pyrimidine-2,4,6-trione lead structure RO 28-2653 (**1**) were synthesized, and their MMP inhibition potency was evaluated in vitro. The radiosynthesis and the in vivo biodistribution of the first ^{18}F-labeled prototype, MMP-targeted tracer [^{18}F]**26**, suitable for molecular imaging by means of positron emission tomography (PET) were realized.

Introduction

Molecular imaging of locally up-regulated and activated extracellular matrix (ECM)-degrading peptidases in vivo, such as matrix metalloproteinases (MMPs), is a clinical challenge. MMPs have been implicated in the proteolytic degradation of ECM components, but are also capable of processing and initiating the release of bioactive molecules, such as growth factors, proteinase inhibitors, cytokines and chemokines.[1] MMPs are subdivided into collagenases, gelatinases, stromelysins and matrilysins, according to common structural elements and substrate specificities. Another subclass of the MMPs is represented by the membrane-type MMPs (MT-MMPs).[2,3] In pathophysiological processes, an increased cytokine and growth-factor-stimulated MMP-gene transcription, followed by an abnormal pro-MMP secretion and zymogen activation, might become prevalent, triggering the progression of inflammation, cancer or cardiovascular diseases, such as atherosclerosis.[1,4–10]

In 2004, our group succeeded in the development of an ^{123}I-labeled nonselective high-affinity MMP-targeted radiotracer based on the hydroxamic acid-based MMP inhibitor CGS 27023A.[11,12] The hydroxamate moiety of CGS27023A functions as zinc-binding group and chelates the zinc ion of the MMP active site. Using the corresponding nonpeptidic radioligand and planar scintigraphy, local MMP activity was specifically imaged in apolipoprotein E-deficient (ApoE$^{-/-}$) mice that develop macrophage- and MMP-rich vascular lesions after carotid artery ligation and cholesterol-rich diet. For the first time, this study highlighted the feasibility of imaging activated MMPs in vivo and emphasized the value of radiolabeled MMPIs for noninvasive scintigraphic in vivo visualization of MMP-related diseases. This was also verified by a recent study, which succeeded in the visualization of endothelial injury-induced MMP activity in vascular remodeling.[13,14] The hydroxamic acid-based broad-spectrum MMP inhibitor ^{111}In-RP782 was applied in combination with microSPECT/CT in an ApoE$^{-/-}$ mouse model of carotid artery injury. An increased and specific tracer uptake was observed in the arterial wall of the guidewire-injured left common carotid artery. MicroSPECT imaging and CT angiography precisely located the MMP-rich lesion within the artery.[15]

Because of the inferior selectivity profile of hydroxamates, a new trend can be recognized in contemporary MMPI design in proceeding from inhibitors with a broad inhibition spectrum to subtype-selective hydroxamate and non-hydroxamate representatives.[16–19] Further shortcomings experienced with typical hydroxamates, such as metabolic instability and high transition-metal binding potential—and thus possible interactions with the metals of other metalloproteases—might additionally be avoided. Pyrimidine-2,4,6-triones (barbiturates) based on

[a] *Dr. H.-J. Breyholz, Dr. S. Wagner, Dr. A. Faust, Prof. Dr. B. Riemann, Prof. Dr. O. Schober, Priv.-Doz. Dr. K. Kopka*
Department of Nuclear Medicine, University of Münster
Albert-Schweitzer-Str. 33, 48149 Münster (Germany)
Fax: (+49) 251-83-47363
E-mail: breyholz@uni-muenster.de

[b] *Dr. C. Höltke*
Department of Clinical Radiology, University of Münster
Albert-Schweitzer-Str. 33, 48149 Münster (Germany)

[c] *Dr. S. Hermann, Prof. Dr. M. Schäfers*
European Institute for Molecular Imaging (EIMI), University of Münster
Mendelstr. 11, 48149 Münster (Germany)

[d] *Prof. Dr. M. Schäfers, Priv.-Doz. Dr. K. Kopka*
Interdisciplinary Center of Clinical Research (IZKF) Münster (Germany)

Supporting information for this article is available on the WWW under http://dx.doi.org/10.1002/cmdc.201000013.

the lead structure of RO 28-2653 (**1**; Figure 1) are prominent examples of such non-hydroxamate MMPIs, exhibiting specific activities for subgroups of secreted MMPs, including the gelatinases A (MMP-2) and B (MMP-9), neutrophil collagenase (MMP-8), as well as the membrane-bound MMPs: MT-1-MMP (MMP-14) and MT-3-MMP (MMP-16).[20–23]

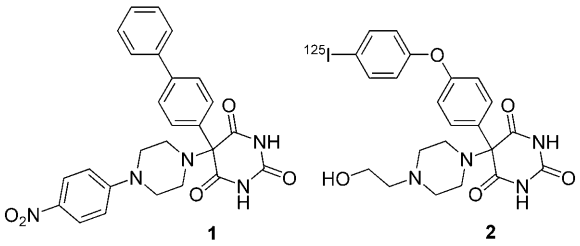

Figure 1. Structures of RO 28-2653 (**1**) and preclinical research tracer **2**.[25]

The selective targeting of MMP-2, MMP-9 and MMP-14 may help to visualize tumor angiogenesis, since these three enzymes are most consistently detected in malignant tissues and are associated with tumor aggressiveness, metastatic potential, and poor prognosis.[6,24] Furthermore, RO 28-2653 was found to exhibit strong antitumor and antiangiogenic efficacy and thus is able to target MMP-rich tumor tissues.[23] These prerequisites support the approach of using barbiturates as molecular imaging agents.

Therefore, in recent years we started exploiting derivatives of RO 28-2653 as a new class of potential selective MMPI radiotracers, resulting in compound **2** (Figure 1), a preclinical research tracer[25] of the first generation, radio-iodinated by [^{125}I]iodine. In more recent studies,[26,27] the amino precursor **29** (shown later in Scheme 6) was conjugated to the near-infrared fluorescent (NIRF) dye Cy 5.5-NHS ester via a short polyethylene glycol ('mini-PEG') linker to give a barbiturate-based NIRF imaging agent, the first of its kind to have been developed so far. MMP-positive tumor xenografts could be successfully visualized in tumor-bearing mice 1–2 h post injection (p.i.) by optical techniques, using this novel imaging agent.

Having successfully proven the feasibility of the chosen approach, herein, we outline the progress of our continuing work towards the development of an MMP imaging agent, based on RO 28-2653, designed for preclinical and clinical imaging. Three exemplary mini-PEG-spaced, fluoro-PEGylated compounds were synthesized as non-radioactive analogues of PET-compatible MMPI radiotracers **26** ($n=1$), **31** ($n=4$) and **38** ($n=8$), where n is the number of ethylene glycol (EG) units in the spacer). All of these lipophilicity-reduced compounds retained good to excellent MMP inhibitory activity. The radiosynthesis and the in vivo biodistribution of [^{18}F]**26** are reported.

Results

Synthesis of the piperazines

Piperazines **6**, **9**–**11**, **14**, **18** and **21**, required for the synthesis of pyrimidine-2,4,6-triones **25**–**32**, were prepared as described in Schemes 1–5.

N-(2-Fluoroethyl)piperazine (**6**) was prepared as the trifluoroacetic acid (TFA) salt by the reaction of *N*-Boc piperazine (**4**)[26] with 2-fluoroethyl tosylate (**5**). Removal of the Boc group was achieved with TFA to give compound **6** in 46% yield (Scheme 1).

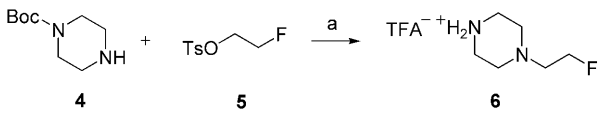

Scheme 1. Synthesis of piperazine derivative **6**. *Reagents and conditions*: a) 1. Cs_2CO_3, DMF, RT, 2 d, 33%; 2. 50% TFA in CH_2Cl_2, RT, o/n, 46%.

Bromo derivative **9** was prepared from tetraethylene glycol (**7**) (Scheme 2), which was first converted to the ditosylate and then heated in the presence of lithium bromide to give dibromide **8**. Coupling with piperazine **4** (similar to the synthesis of **6**) was accomplished in 40% yield. Cleavage of the Boc group gave **9** in 47% yield.

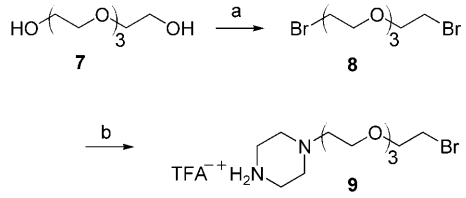

Scheme 2. Synthesis of piperazine derivative **9**. *Reagents and conditions*: a) 1. TsCl, Et_3N, CH_3CN, RT, 20 h, 85%; 2. LiBr, acetone, reflux, o/n, 69%; b) 1. **4**, Cs_2CO_3, DMF, RT, 2 d, 40%; 2. 50% TFA in CH_2Cl_2, RT, o/n, 47%.

Azide **10** and amino derivative **11** (shown later in Scheme 6) were prepared according to our previously described procedures.[26] Hydroxy derivative **14** was synthesized by reaction of **7** with one equivalent triphenylmethanol (Scheme 3). Subse-

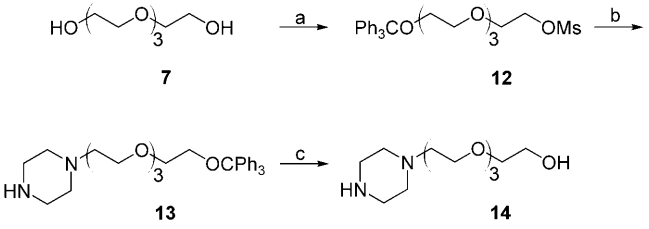

Scheme 3. Synthesis of piperazine derivative **14**. *Reagents and conditions*: a) 1. Ph_3COH, $TsOH{\cdot}H_2O$, toluene, reflux, 2 h; 2. MsCl, Et_3N, CH_2Cl_2, 0 °C→RT, o/n, 97%;[28] b) piperazine (**3**), Cs_2CO_3, DMF, 100 °C, 2 d, 86%; c) HCl, MeOH, RT, 16 h, 56%.

quent mesylation yielded **12**,[28] which was coupled to piperazine (**3**) in DMF to give **13**. Finally the trityl protecting group of **13** was removed to yield the target compound **14**.

Fluoro derivative **18** was prepared as shown in Scheme 4. Triethylene glycol (**15**) was converted into the corresponding tritylether and subsequently reacted with 2-fluoroethyl tosylate

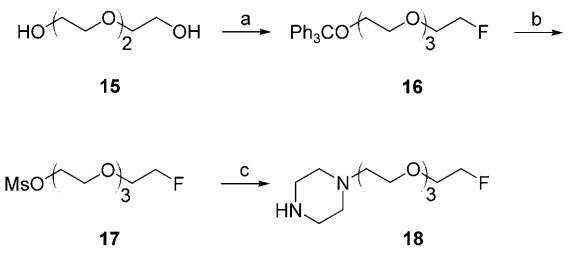

Scheme 4. Synthesis of piperazine derivative **18**. *Reagents and conditions*: a) 1. Ph_3COH, $TsOH{\cdot}H_2O$, toluene, reflux, 2 h; 2. 2-fluoroethyl tosylate (**5**), *t*BuOK, *t*BuOH, reflux, 24 h, 54%; b) 1. $TsOH{\cdot}H_2O$, MeOH, reflux, 2 h; 2. MsCl, Et_3N, CH_2Cl_2, 0 °C→RT, o/n, 52%; c) Piperazine (**3**), Cs_2CO_3, DMF, 100 °C, 2 d, 94%.

(**5**) to give the fluoro compound **16**. After cleavage of the trityl protecting group and mesylation, intermediate **17** was obtained and coupled to piperazine (**3**) to give the target compound **18**.

The synthesis of alkyne derivative **21** began with the formation of intermediate **12** (Scheme 5). Conversion with propargyl alcohol led to alkyne **19**. Exchange of the trityl group for mesyl was accomplished in 67% yield as described above. Coupling to *N*-Boc piperazine (**4**) and deprotection was performed in 70% and 86% yield, respectively, to give the target compound **21**.

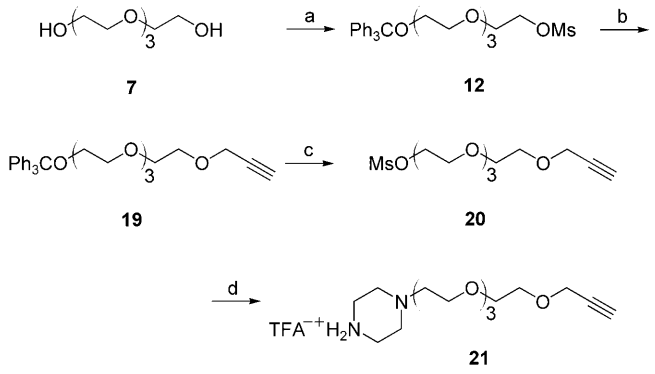

Scheme 5. Synthesis of piperazine derivative **21**. *Reagents and conditions*: a) 1. Ph_3COH, $TsOH{\cdot}H_2O$, RT, 2 h, toluene; 2. MsCl, Et_3N, CH_2Cl_2, RT, o/n, 97%;[28] b) 1. HC≡C-CH-OH, Cs_2CO_3, DMF, 100 °C, 1.5 h, 58%; c) 1. $TsOH{\cdot}H_2O$, MeOH, reflux, 2 h; 2. MsCl, Et_3N, CH_2Cl_2, 0 °C→RT, o/n, 67%; d) 1. **4**, Cs_2CO_3, DMF, RT, 2 d, 70%; 2. 50% TFA in CH_2Cl_2, RT, o/n, 86%.

Synthesis of 5-(4-phenoxyphenyl) pyrimidine-2,4,6-triones 25–32

The 5-(4-phenoxyphenyl) pyrimidine-2,4,6-triones **25**–**32** were prepared from the corresponding piperazines **3**, **6**, **9**–**11**, **14**, **18** or **21**, respectively (Scheme 6). To assemble the barbiturate scaffold, a palladium-catalyzed ($Pd(OAc)_2$) coupling reaction of diisopropyl malonate and 4-bromophenyl phenyl ether (**22**) was used.[29] Condensation of malonic ester **23** with urea, and a one-pot reaction involving the *N*-bromosuccinimide (NBS)-mediated bromination at the 5-position of the pyrimidine-

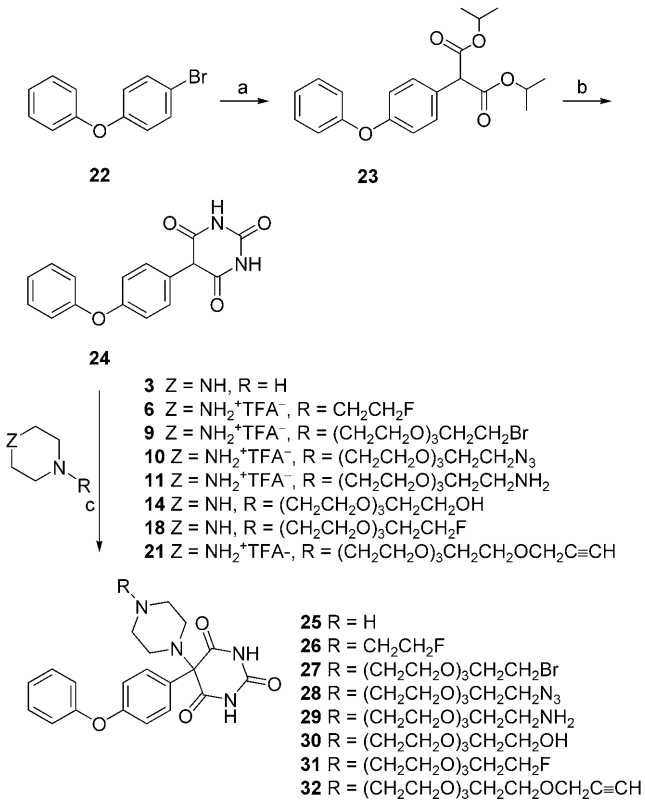

Scheme 6. Syntheses of phenoxyphenyl pyrimidine-2,4,6-triones **25**-**32**. *Reagents and conditions*: a) $Pd(OAc)_2$, tBu_3P, CuF_2, *t*BuONa, diisopropyl malonate, 67 °C, 15 h; b) urea, *t*BuOK, THF, 80 °C, 17 h, 84% (two steps),[29] this work: 30–40%; c) piperazines **3**, **6**, **9**–**11**, **14**, **18** and **21** (1.0 equiv), NBS, K_2CO_3, DMF, 5–10 °C, 2 h then RT, 20 h, 43% (**25**), 45% (**26**) 36% (**27**), 43% (**28**),[26] 71% (**29**),[26] 55% (**30**), 32% (**31**), 78% (**32**).

2,4,6-trione and the introduction of the piperazine subunit, yielded barbiturates **25**–**32** in three steps. Hutchings et al. obtained intermediate **24** in 84% yield (over two steps).[29] The average yield of our preparations ranged between 30 and 40% with a maximum of 62%. Barbiturates **25**–**32** were obtained in yields between 36% and 78%. The overall yields (including the synthesis of the corresponding piperazine derivatives) ranged between 0.5% and 17% for the three- to nine-step syntheses: **25**, 17% (3 steps); **26**, 1% (7 steps); **27**, 9% (7 steps); **28**, 0.8% (8 steps);[26] **29**, 0.6% (8 steps);[26] **30**, 15% (7 steps); **31**, 4% (8 steps); **32**, 6% (9 steps).

Synthesis and in vitro data of pyrimidine-2,4,6-triones 42–45

The 3-bromo-4-methoxy-phenoxyphenyl barbituric acid derivatives **42**–**45** were synthesized as depicted in Scheme 7. Inter-

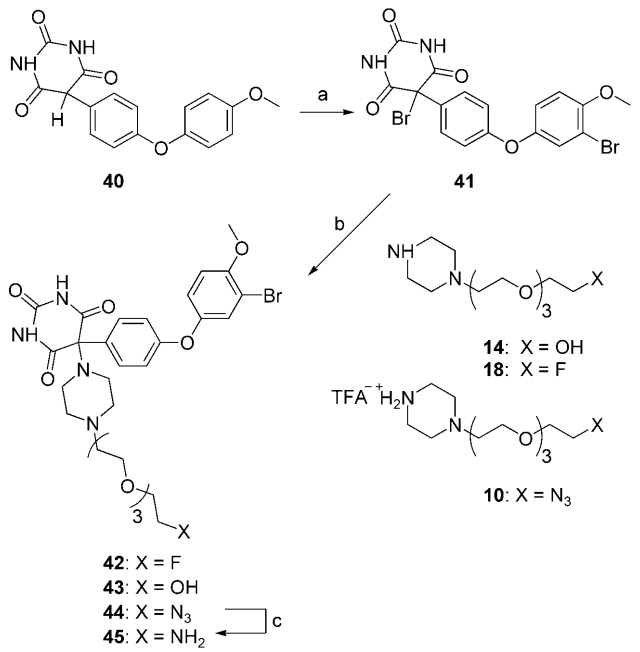

Scheme 7. Syntheses of compounds **41**–**45**. *Reagents and conditions*: a) NBS (1.2 equiv), dibenzoyl peroxide, CCl_4, reflux, 4 h, 58%; b) MeOH, RT, o/n (3.0 equiv Et_3N added for **10**), 30% (**42**), 54% (**43**), 84% (**44**); c) H_2, Pd/C, EtOAc, RT, 16 h, 54%.

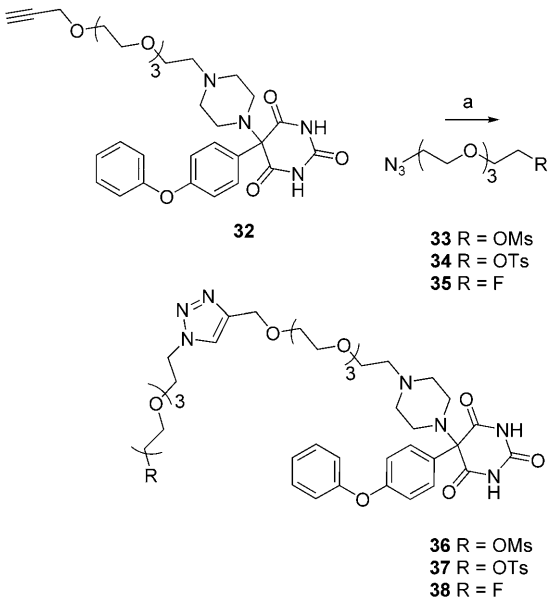

Scheme 8. Synthesis of the 1,2,3-triazoles **36**–**38**. *Reagents and conditions*: a) azides **33**, **34** or **35** (1.0 equiv), $CuSO_4 \cdot 5H_2O$ (30 mol%), sodium ascorbate (40 mol%), *t*BuOH/H_2O (4:1), RT, o/n, 19% (**36**), 30% (**37**), 32% (**38**).

mediate **40**[25] was intended to be brominated at the barbituric acid 5-position by using NBS and dibenzoyl peroxide in tetrachloromethane. However, instead of one bromine—as expected and demonstrated in our previous work[25]—two bromine atoms were introduced to give the dibromo product **41** in 58% yield. One bromine was incorporated at the aliphatic 5-position and the other at the anisole ring, *ortho* to the methoxy group, as demonstrated by two-dimensional NMR and NOE experiments (see Supporting Information). Compound **41** was reacted with piperazines **14** and **18** (Schemes 3 and 4) in methanol to generate the fluoro derivative **42** (yield: 30%) and the and hydroxy derivative **43** (yield: 54%). In case of the TFA salt **10**, three equivalents of triethylamine were added to the reaction mixture to give azide **44** in 84% yield. The azide was subsequently reduced by catalytic hydrogenation to give amine **45** in moderate conversion.

Synthesis of the triazoles 36–38

Pyrimidine-2,4,6-trione **32** was used as the alkyne component in a copper(I)-catalyzed, 1,3-dipolar Huisgen cycloaddition using azides **33**, **34** or **35**, respectively. The click reaction was realized in a solvent mixture of *t*BuOH and water containing the catalytic system sodium ascorbate and copper sulfate pentahydrate at room temperature (see Scheme 8). The 1,4-disubstituted 1,2,3-triazole click products **36**–**38** were formed in yields ranging from 19% to 32% (see Experimental Section for further details).

The overall yields for this twelve- to thirteen-step procedures ranged between 0.3% and 0.5% (0.3% (**36**), 0.5% (**37**), 0.4% (**38**)). The by-product (**30**) of all click reactions (Scheme 6), as identified by analytical HPLC and MS (see Experimental section) turned out to be inseparable from the main products **36**–**38** by silica gel column chromatography. Therefore, the 1,2,3-triazoles were isolated by preparative HLPC. The synthesis of the azides **33**–**35** is outlined in Scheme 9. Tetraethylene glycol

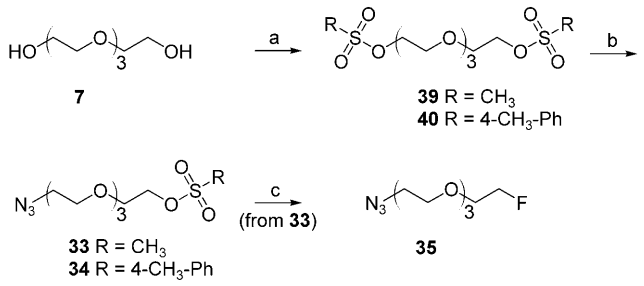

Scheme 9. Mini-PEG intermediates **33**, **34** and **35**, synthesized as azide components for 1,3-dipolar cycloadditions leading to 1,2,3-triazoles **36**–**38**. *Reagents and conditions*: a) MsCl or TsCl, Et_3N, CH_2Cl_2, RT, 20 h, 85% (**39**),[26] 80% (**40**); b) NaN_3, CH_3CN, 120 °C, 5 h, 36% (**33**),[26] 34% (**34**); c) TBAF (1 M) in THF, reflux (2 h)→RT (o/n), 78%.

(**7**) was subjected either to twofold mesylation or tosylation, resulting in the dimesylate **39** or ditosylate **40**, respectively, which were then converted to the mono azides **33** and **34**. Mesylate **33** was subsequently submitted to fluorination by tetra-*n*-butylammonium fluoride to give the fluorinated azide **35**.

Enzyme assays and log *D* values

The MMP inhibition potencies of the barbituric acid derivatives **25**–**32**, **38** and **42**–**46** were measured in fluorogenic in vitro in-

hibition assays as described previously.[30] The resulting IC_{50} values for the investigated MMPs were calculated from a nonlinear regression fit of the concentration-dependent reaction rates. The results are displayed in Table 1, which also contains

Table 1. Inhibition of various MMPs by the pyrimidine-2,4,6-triones **25**–**32**, **38**, and **42**–**46** with corresponding log *D* values.

Compd	IC_{50} [nM][a]				clog *D*[b]
	MMP-2	MMP-8	MMP-9	MMP-13	
25[c]	37±3	58±8	44±5	83±4	2.62
26[d]	23±9	138±12	7±2	645±17	2.88[e]
27	10±4	55±24	13±8	207±22	2.54
28[f]	38±1	71±8	10±4	57±12	1.84
29	31±3	118±10	85±14	177±20	−0.34
30	70±14	122±56	6±2	333±60	0.84
31	62±5	108±7	93±6	86±4	1.72
32	32±15	91±25	52±4	77±7	1.75
38	81±6	80±30	75±5	237±32	0.67
42	292±53	395±42	36±18	2950±360	1.84
43	259±102	600±233	928±262	5480±970	0.96
44	136±20	n.d.	157±65	n.d.	1.97
45	240±75	n.d.	864±217	n.d.	−0.22
46	23±5	146±48	17±5	28±11	2.99

[a] Values are the mean ±SD of three experiments. [b] calculated log *D* (clog *D*) values were calculated by ACD/Chemsketch version ACD/Labs 6.00 (clog *D* = clog *P* at physiological pH (7.4) with consideration of charged species). [c] IC_{50} (MMP-14) = 37±3 nM [d] IC_{50} (MMP-1) > 50 μM, IC_{50} (MMP-3) = 760 μM. [e] Experimental log *D* = 2.15±0.02. [f] IC_{50} (MMP-14) = 120±18 nM. n.d. = not determined.

the calculated log *D* values (clog *D*) to indicate the changes in lipophilicity caused by the structural modifications. Additionally, the log *D* value of the key radioligand [^{18}F]**26** was determined experimentally. The calculated and experimental log *D* values differ by 0.73 log *D* units (clog *D* (**26**) = 2.88 compared with experimental log *D* ([^{18}F]**26**) = 2.15).

All unlabeled analogues of tracer candidates **26**, **31** and **38** retained good MMP inhibition potencies. A detailed reflection on the IC_{50} values can be found in the discussion section. Because of its higher gelatinase selectivity, derivative **26** appeared to be an ideal starting point for the radiosynthesis of the corresponding fluoroethyl tracer [^{18}F]**26**. Its radiosynthesis is described in the following paragraph. Our current research focus is on the realization of PEGylated tracer variants [^{18}F]**31** (PEG = 4 EG units) and [^{18}F]**38** (PEG = 8 EG units).

Radiosynthesis of fluorinated pyrimidne-2,4,6-trione

The radiosynthesis of the barbituric acid-based [^{18}F]fluoroethyl radioligand [^{18}F]**26** is shown in Scheme 10. This semi-automated two-step procedure starts with the synthesis of 1-[^{18}F]fluoro-2-tosyloxyethane [^{18}F]**5** from ethylene glycol di-*p*-tosylate and [^{18}F]K(K_{222})F. [^{18}F]**5** was obtained in a radiochemical yield of 53.3±2.3% (decay-corrected, *n* = 6). The second step was performed outside the automated synthesizer. [^{18}F]**5** was coupled to the piperazine moiety of precursor **25** by heating in dimethyl sulfoxide. [^{18}F]**26** was produced in a radiochemical yield of 21.3±4.0% (decay-corrected, *n* = 6). The overall radiochemical yield of this two-step radiosynthesis was 11.3±2.2% (decay-corrected, based on cyclotron-derived [^{18}F]fluoride ions). The radiochemical purity was 98.5±1.5% after 142±12 min from the end of radionuclide production. The determined specific radioactivities were 23±10 GBq μmol^{-1} at the end of radiosynthesis (*n* = 6).

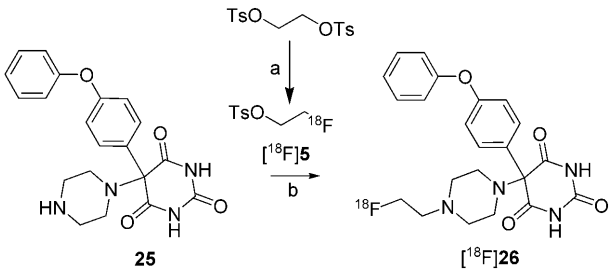

Scheme 10. Two-step radiosynthesis of [^{18}F]fluoroethyl radioligand [^{18}F]**26** as a potentially PET-compatible barbituric acid-derived MMP-targeted imaging probe. *Reagents and conditions*: a) [^{18}F]K(K_{222})F, K_2CO_3, CH_3CN, 84 °C, 4 min; b) DMSO, 120 °C, 15 min.

The PET-compatible PEG_4-tracer variant [^{18}F]**31** can be prepared by direct radiofluorination of the tosylate precursor, which could be generated either from the bromo derivative **27** (e.g., by reaction with silver tosylate) or the hydroxy derivative **30** (e.g., by reaction with tosyl chloride and pyridine). Approaches to realize this lipophilictiy-reduced tracer variant (clog *D* (**31**) = 1.72 versus clog *D* (**26**) = 2.88) are currently underway. Different strategies for the radiosynthesis of PET-compatible PEG_8-tracer variant [^{18}F]**38** can be conceived. Starting from precursors **28** or **32**, the radiosynthesis of [^{18}F]**38** might be performed either as two-step- or as one-pot reaction, i. e. radiofluorination of labeling synthons, such as **33** or **34**, giving the ^{18}F-labeled building block [^{18}F]**35**. This intermediate could then be used for subsequent 1,2,3-triazole formation in the same reaction vessel without intermediate purification.[31] Alternatively, direct one-step radiofluorination of precursors already containing the 1,2,3-triazole moiety, such as **36** or **37**, might also be feasible. Regarding the one-pot procedure, only traces of [^{18}F]**38** could be isolated thus far, most likely because a intramolecular cyclization product (see Discussion section and scheme S1 in the Supporting Information) was formed. To circumvent this unintended side reaction, we are currently investigating the two-step process for the generation of [^{18}F]**38**, i.e., via click reaction between alkyne **32** and azide [^{18}F]**35**. According to calculated log *D* values, [^{18}F]**38** should be more hydrophilic by more than two log *D* units (clog *D* (**38**) = 0.67 versus clog *D* (**26**) = 2.88) compared to non-PEG_8-PEGlyated derivative **26**.

Biodistribution

For biodistribution studies, adult C57/BL6 mice were intravenously injected with the prototype MMP-targeted radiotracer [^{18}F]**26**. Shortly after completion of the [^{18}F]**26** scan (5 min), the PET tracer 2-deoxy-2-[^{18}F]fluoro-D-glucose ([^{18}F]FDG) was additionally injected via the tail vein to outline the left ventricular

myocardium for placement of an arterial region-of-interest (ROI).

Dynamic PET scans were performed throughout the studies and reconstructed in to images at different time points after injection of [^{18}F]**26** and [^{18}F]FDG (Figure 2). The coronal whole-body small-animal PET images showed that the tracer uptake in nontarget organs, such as the brain, lung, heart and muscle, was low over all time points. The initial liver radioactivity 5–10 min after injection of [^{18}F]**26** was high but rapidly decreased up to 90–120 min p.i. There was also notable uptake in the bladder, indicative of a predominantly renal excretion with some hepatobilliary clearance. The low accumulation of [^{18}F]**26** in the skeleton suggests that the extent of tracer defluorination and generation of free [^{18}F]fluoride is negligible. Figure 3 shows the averaged time–activity curves (TACs) for tissues involved with metabolic and excretory processes (bladder, kidney, liver and small/large bowel; Figure 3 A) and for possible target tissues (brain, lung and muscle; Figure 3 B) where dysregulated MMP activity might occur in MMP-associated diseases.

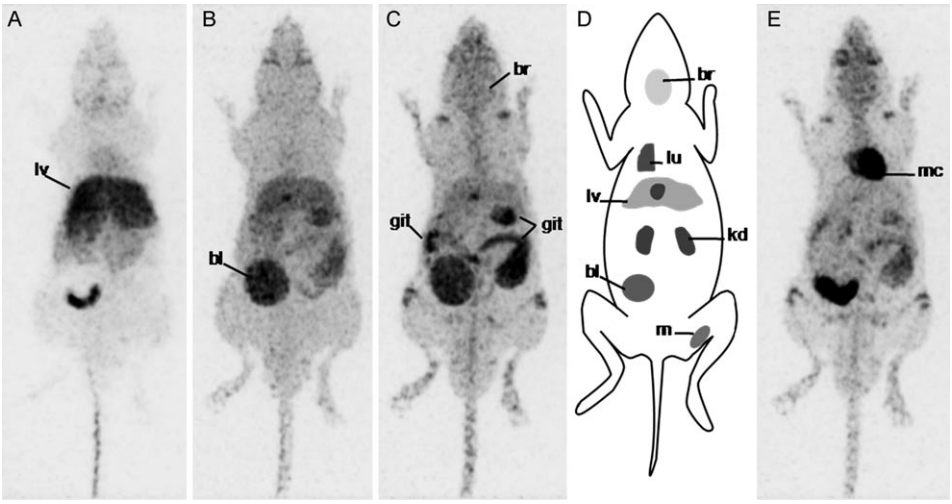

Figure 2. Biodistribution of radioactivity in an adult C57/BL6 mouse after intravenous injection of [^{18}F]**26** and [^{18}F]FDG visualized by small-animal PET. Panels A–C and E show maximum intensity projections. PET scans 5–10 min (panel A), 30–60 min (panel B) and 90–120 min (panel C) after injection of [^{18}F]**26** are displayed. Panel D: ROI overview. Panel E: [^{18}F]FDG scan after completion of the [^{18}F]**26** scan. Labeled structures: liver (lv), bladder (bl), kidneys (kd), gastrointestinal tract (git), brain (br), lung (lu), muscle (m), myocardium (mc).

The data were determined from a multiple time-point PET study and demonstrate the favorable pharmacokinetic behavior of model tracer [^{18}F]**26**, corresponding to the physical half-life of the positron emitter ^{18}F (~110 min).

Discussion

Prerequisites

Based on the work of Grams et al.[20,21] and Foley et al.[22], who introduced pyrimidine-2,4,6-triones, such as RO 28-2653 (Figure 1), as a new class of non-hydroxamate small-molecule MMP inhibitors, we modified this lead structure to gain access to a complete set of four pairs of precursors/non-radioactive analogues (reference compounds) of prospective radiotracers that may be useful for the in vivo imaging of locally up-regulated and activated MMPs by means of SPECT or PET.[25] We have suggested a radioiodinated variant **2** (Figure 1), labeled with the radionuclide [^{125}I]iodine, as a model compound for in vitro and ex vivo applications.

Our ongoing research efforts are now aimed at the design of radiofluorinated variants of model tracer **2** for preclinical and clinical PET studies. In particular, we aim to increase the hydrophilicity and water solubility of the commonly lipophilic barbiturates, which are known to be highly metabolically stable, to reduce plasma-protein binding. Finally, efforts will be made to direct the pharmacokinetics of the modified radiolabeled derivatives towards early and high in vivo target-to-background ratios of the radiotracer-associated scintigraphic signal.

Tracer modification strategy

PEGylation with polyethylene glycol (PEG) units, consisting of several thousands of daltons, is known to significantly influence the pharmacokinetic behavior of a drug.[32] Another approach involves the conjugation of drugs with short PEG chains, containing only a few PEG units (mini-PEGs), which increase the hydrophilicity and the water solubility and can direct the tracer towards the renal excretion route. This would result in a higher signal-to-noise ratio of the tracer accumulation in target tissues compared to the non-PEGylated derivatives. This approach has been successfully shown in other radiopharmaceutical studies on peptides[33,34] and small-molecule (nonpeptide) drugs.[35,36]

We have recently shown that by introducing the NIRF dye Cy 5.5 into the mini-PEGylated precursor **29** (see Scheme 6 for structure) a dramatic increase of water solubility, achieved here by introducing negative charges into the molecule, can be a crucial element in the design of barbiturate-based MMP-targeted tracers.[26,27] As MMPs act in the extracellular space, water-soluble MMPIs should reach and interact with their biological target more efficiently, show a reduced intracellular MMPI accumulation and consequently reduced interaction with metalloenzymes, which are abundant in cells.

Consequently, we fixed the 5-(4-phenoxyphenyl) substituent and initially introduced the mini-PEG spacer with four EG units at the piperazine unit, which appeared to be an ideal PEGylation site since it functions as a P_2' substituent directed towards the solvent-exposed S_2' pocket of the enzyme. This allows an arbitrary elongation of the PEG chains of azide **28** and alkyne **32**, which may be optionally elongated by attaching PEG moi-

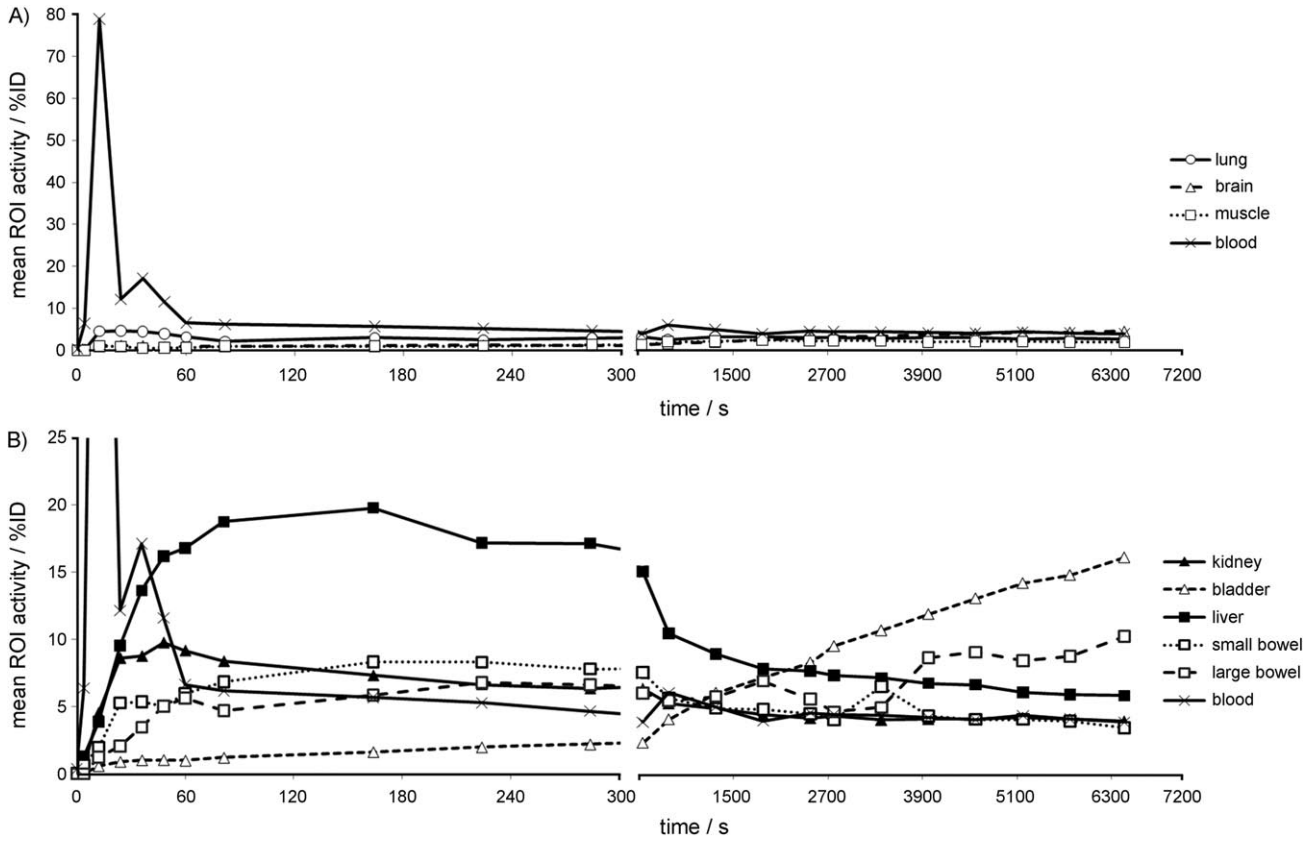

Figure 3. Representative biodistribution of radioactivity in an adult C57/BL6 mouse after intravenous injection of [^{18}F]**26**. A) time–activity curves of the blood, brain, lung and muscle. B) time–activity curves of the blood, bladder, kidney, liver and small/large bowel. ROI: region-of-interest. %ID: % injected dose.

eties with the desired number of EG units using click chemistry. Thus, the effect of the number of the EG units on the pharmacokinetic behavior of the molecule can be explored.

Instead of the hitherto used standard eight-step barbiturate synthesis,[20,25] a much more effective three-step synthesis, proposed by Hutchings et al.[29] was employed for their preparation.

PEG_1- and PEG_4-tracer variants

A series of pyrimidine-2,4,6-triones **25**–**32** and **42**–**46** was synthesized via strategies given in Schemes 6 and 7. These compounds were prepared for the following purposes: Piperazine derivative **25** and fluoroethyl piperazine derivative **26** were synthesized as a labeling precursor and the corresponding non-radioactive analogue of the PET-compatible MMP-targeted radiotracer candidate [^{18}F]**26**, respectively (Scheme 10). A two-step radiosynthesis consisting of the preparation off 1-[^{18}F]fluoro-2-tosyloxyethane ([^{18}F]**5**) and subsequent fluoroethylation of piperazine precursor **25** successfully yielded target compound [^{18}F]**26**. In a conceivable one-step process consisting of the direct nucleophilic radiofluorination of the corresponding tosyl precursor (system: piperazine-CH_2CH_2-OTs), an intramolecular cyclization reaction is likely and accounts for the failure of the synthesis of a toslyate precursor for direct radiofluorination.

With a clog*D* value of 2.88, the fluorinated analogue **26**, which we define as PEG_1-modified derivative, is already four- to five-times more hydrophilic than the first generation iodo radioligand **2** (clog*D* = 3.53). The deviation of the calculated from the experimental log*D* values for compound **26** was approximately 25%. The MMP inhibitory potency of compound **2** (MMP-2, IC_{50} = 7 nM; MMP-9, IC_{50} = 2 nM) was maintained in the modified analogue **26**, which is still a one- to two-digit nanomolar MMP inhibitor of gelatinases (MMP-2, IC_{50} = 23 nM; MMP-9, IC_{50} = 7 nM. Inhibition of MMP-8 and MMP-13 by compound **26** was only observed in the upper nanomolar range. The marked gelatinase selectivity becomes even more apparent when the micromolar IC_{50} values of **26** for the inhibition of MMP-1 and MMP-3 are considered (Table 1). Similar to compound **2**, derivative **26** exhibits a threefold MMP-9 selectivity relative to MMP-2. As might not necessarily be expected, the biodistribution study shows excretion of the PEG_1-variant [^{18}F]**26** through the kidneys with only moderate uptake in, and fast clearance from, the liver (Figures 2 and 3).

The azido derivative **28** and the amino derivative **29** were originally synthesized as intermediate and labeling precursor for the aforementioned MMP-targeted optical imaging probe.[26] Beyond this application, we intend to use azide **28** in further click approaches, and amine **29** for coupling reactions with radionuclide-containing prosthetic groups (such as *N*-succinimidyl-4-[^{18}F]-fluorobenzoate, [^{18}F]SFB). As depicted in

Table 1, the introduction of the PEG_4 chain is well tolerated in **28** and **29** in terms of retained MMP inhibitory potencies. Compounds **28** (IC_{50} values: 10–71 nM) and **29** (IC_{50} values: 31–177 nM) represent two- and two- to three-digit nanomolar MMP inhibitors, respectively. Azido compound **28** displayed a 1.5 to twofold MMP-2 selectivity (versus MMP-8 and MMP-13) and a six- to sevenfold MMP-9 selectivity (versus MMP-8 and MMP-13). Amino derivative **29** displayed a four- to sixfold MMP-2 selectivity (versus MMP-8 and MMP-13) and a 1.5- to twofold MMP-9 selectivity (versus MMP-8 and MMP-13). Compound **28** showed a threefold selectivity for MMP-9 relative to MMP-2, similar to compound **26**. In contrast, compound **29** exhibited a threefold MMP-2 selectivity relative to MMP-9.

The PEG_4-variants **27** (bromo derivative) and **30** (hydroxy derivative) were prepared to serve as advanced intermediates (one step each) to realize a tosyl precursor for radiofluorination, which might ultimately result in the PET-compatible PEG_4-tracer variant [^{18}F]**31**. Both intermediates **27** and **30** also showed notable gelatinase selectivity relative to MMP-8 and MMP-13 (Table 1).

Considering the clog*D* values of the PEG_4-variant **31** (clog*D* = 1.72) and PEG_1-variant **26** (clog*D* = 2.88), we succeeded to further reduce the lipophilicity of the fluorinated mini-PEG-barbiturates by more than one log*D* unit (14-fold). Using compounds **42**–**46**, further fluoro-, hydroxy-, azido- and amino-functionalized PEG_4 derivatives were prepared, bearing bromo, iodo or methoxy groups, respectively, at the 3- and/or 4-(4-phenoxyphenyl) positions.

PEG_8-tracer variant by click approach

Like azide **28**, alkyne **32** allows for the application of the copper(I)-catalyzed 1,3-dipolar Huisgen cycloaddition (click reaction[37–40]) to generate 1,4-disubstituted 1,2,3-triazoles, such as **36**–**38**, by reaction with azides **33**–**35** (Scheme 8). The 1,2,3-triazole unit has been shown to possess some valuable characteristics with respect to the intended in vivo application. Apart from its function as a linker, it is also able to act as part of a pharmacophore. As such, it can contribute to the binding of the molecule to biological targets through hydrogen-bonding, dipole (dipole moment > 5 D) and π-stacking interactions.[41,42] Furthermore, it can improve pharmacokinetic parameters, hydrophilicity and solubility beyond the level achieved by PEGylation alone. Moreover, 1,2,3-triazoles are relatively robust towards metabolic degradation.

The number of studies on bioactive molecules that are labeled with [^{18}F]fluoro-PEGylated radiosynthons by click chemistry[43] is increasing continuously. Recently, Chen et al. successfully applied a similar click chemistry approach by labeling an RGD peptide with a [^{18}F]fluoro-PEG_3 spacer, yielding the tracer ^{18}F-FTPA-RGD2. Preclinical microPET studies using tumor-bearing mice with an increased $\alpha_v\beta_3$ integrin density in the tumor tissue showed that the tracer displayed good tumor-targeting efficacy, metabolic stability, as well as favorable in vivo pharmacokinetics (i.e., predominantly renal excretion, fast clearance rate, low liver uptake).[44]

By using this click approach, the formal PEG_8 derivatives **36** and **37** (mesyl-/tosyl-radiofluorination precursors), as well as the unlabeled analogue **38** of the intended PET-compatible MMP-targeted imaging probe, could easily be prepared (Scheme 8 and 9). A further significant log*D* shift of one log*D* unit (tenfold) was accomplished by the 'transition' from derivative **31** to **38** (Table 1). This enhancement in hydrophilicity can be explained by a synergistic effect arising from both, PEGylation and triazole formation (see above). The MMP inhibition profiles of **31** and **38** are similar in that both fluoro-PEGylated compounds retain acceptable MMP inhibitory potencies. However, the MMP selectivity profile, as shown for compound **26**, is completely lost in both PEGylated compounds (Table 1).

Radiosyntheses were initiated to achieve the radiofluorinated analogue of **38**, [^{18}F]**38**. Unfortunately, due to nearly identical HPLC retention times of the mesylate precursor **36** and the non-radioactive tracer analogue **38** under the chosen HPLC-conditions (data not shown), mesylate **36** emerged as an unsuitable precursor for the radiofluorination of the PEG_8 variant [^{18}F]**38**. Therefore, the tosyl precursor **37**, showing a different HPLC retention time compared with **38**, was applied in preliminary radiosynthesis approaches. The HPLC-purification step was then feasible, however, only traces of the desired radiolabeled product [^{18}F]**38** were obtained. A major non-radioactive by-product was isolated by HPLC. We hypothesize, based on mass spectrometry data ($[M]^+ = 796$ Da), that a rearrangement product (see compound **39** in scheme S1 of the Supporting Information) is formed by intramolecular ring closure either at the pyrimidine-2,4,6-trione oxygen or nitrogen. Future refinement of the radiofluorination conditions; for example, the exchange of the [^{18}F]K(K_{222})F system for [^{18}F]TBAF, is aimed at the suppression of this undesired side reaction, which may arise from a template effect of the potassium ion.

Conclusions

Three mini-PEG-spaced, fluoro-PEGylated non-radioactive analogues of barbituric acid-based PET-compatible MMP-targeted radiotracers **26** ($n = 1$), **31** ($n = 4$) and **38** ($n = 8$) (n = number of EG units) have been synthesized to systematically explore the effect of PEGylation on the lipophilicity, as well as MMP inhibitory potency and MMP-subgroup selectivity of the resulting barbiturate-based MMP inhibitors. A two-step-radiosynthesis of [^{18}F]**26** ($n = 1$), which in analogy to model tracer **2** was found to be a highly potent and gelatinase-selective tracer candidate, was successfully established.

Preliminary biodistribution studies of [^{18}F]**26** indicated that there was no tissue specific accumulation in wild-type mice. The clearance of any ^{18}F-labeled radiotracer candidate from a living subject should correspond with the physical half-life of the PET radionuclide ($t_{\frac{1}{2}} = 109.7$ min), which is indeed realized in the case of model tracer [^{18}F]**26**, warranting its future evaluation in various murine models displaying pathological MMP dysregulation. Low uptake in the normal state is advantageous for the study of locally enhanced MMP activity in the diseased state. The non-radioactive analogues of the PEGylated tracer variants **31** ($n = 4$) and **38** ($n = 8$) maintained a high MMP in-

hibitory potency, however, at the expense of MMP-subgroup selectivity, which was still found for derivative **26** ($n=1$). Advanced precursors (e.g., **32** and **37**) were prepared, but further work remains necessary to ultimately establish corresponding radiolabeling procedures for the preparation of the [^{18}F]fluoro-PEG_4- and -PEG_8-ylated variants of barbiturate-based MMP-targeted radioligands.

Finally, the approach of barbiturate-based MMP-targeted radiotracers considered here should be applicable in noninvasive in vivo imaging of MMP-2 and MMP-9-associated diseases by means of PET, ideally in combination with the necessary morphological overlay for precise anatomic localization of the molecular signal, which is nowadays realized by the state-of-the-art hybrid imaging systems, such as PET-CT and MR-PET.

Experimental Section

Chemistry

General Methods: All chemicals, reagents and solvents for the synthesis of the compounds were analytical grade, purchased from commercial sources and used without further purification, unless otherwise specified. Melting points were determined in capillary tubes on a Stuart Scientific SMP3 capillary melting point apparatus and are uncorrected. ^{1}H NMR, ^{13}C NMR and ^{19}F NMR spectra were recorded on Bruker ARX 300 and/or AMX 400 spectrometers. Two-dimensional and NOE-NMR spectra were determined on a Varian 600 MHz Unity Plus instrument. $CDCl_3$ contained tetramethylsilane (TMS) as an internal standard. Mass spectra were obtained on a Varian MAT 212 (EI = 70 eV) spectrometer and a Bruker MALDI-TOF-MS Reflex IV instrument (matrix: DHB). Exact mass analyses were conducted on a Waters Quattro LC and a Bruker MicroTof apparatus. Elemental analyses were carried out on a Vario EL III analyzer. All aforementioned spectroscopic and analytical investigations were done by staff members of the Institute of Organic Chemistry, University of Münster (Germany). All compound purifications and determinations of purity by HPLC were performed using a Knauer gradient RP-HPLC system, equipped with two K-1800 pumps, an S-2500 UV detector and RP-HPLC Nucleosil Eurosphere 100–10 C-18 columns for analytical (250 mm × 4.6 mm), semipreparative (250 mm × 8 mm) and preparative (250 mm × 20 mm) purposes (unless specified otherwise). The following eluents were used: eluent A: water (0.1% TFA), eluent B: acetonitrile (0.1% TFA) (unless specified otherwise). The following conditions were used (unless specified otherwise):

a) *analytical*: 90% A→20% A (30 min), 20% A (5 min), 20% A→90% A (5 min); flow rate = 1.5 mL min^{-1}; detection at $\lambda = 254$ nm. b) *semipreparative*: 90% A→20% A (17 min), 20% A (2.5 min), 20% A→90% A (1.5 min); flow rate = 5.5 mL min^{-1}; detection at $\lambda = 254$ nm. c) *preparative*: 80% A→30% A (12 min), 30% A (1 min); flow rate = 18.5 mL min^{-1}; detection at $\lambda = 254$ nm.

Preparation of piperazine derivatives: Compounds **10** and **11** were prepared according to previously described procedures.[25] Piperazine derivates **14** and **18** were prepared as specified below. The piperazinium trifluoroacetates **6**, **9** and **21** were prepared following this general procedure: *N*-Boc piperazine (**4**)[26] (1.45 equiv) was added to a solution of 2-fluoroethyl tosylate (**5**) (prepared by adding TsCl to a solution of 2-fluoroethanol in pyridine), compound **8** (see Supporting Information) or mesylate **20** (see Supporting Information) and Cs_2CO_3 (1 equiv) in dry DMF (10 mL mmol^{-1}). After stirring at RT for 2 d, water was added and the mixture was extracted with CH_2Cl_2 (3×). The combined organic extracts were washed with brine (1×), dried (Mg_2SO_4), filtered and concentrated in vacuo. Purification by silica gel chromatography gave the *N*-Boc-protected piperazines: EtOAc/cyclohexane, 2:1 (**6**); EtOAc/MeOH, 19:1 (**9**); EtOAc/MeOH, 2:1 (**21**). The reaction products were then subjected to *N*-Boc removal by action of an excess of 50% TFA in CH_2Cl_2. The mixture was stirred at RT overnight and finally evaporated to remove the excess of TFA. Purification by silica gel column chromatography (EtOAc/MeOH, 2:1) gave piperazinium trifluoroacetates **6**, **9** and **21**.

4-(2-Fluoroethyl)piperazin-1-ium trifluoroacetate (6): *N-Boc-protected intermediate*: yield = 33%, yellow oil; ^{1}H NMR (300 MHz, $CDCl_3$): $\delta = 4.57$ (dt, $^2J_{H,F} = 47.9$ Hz, $^3J = 4.9$ Hz, 2H, *N*-CH_2CH_2F), 3.45 (t, $^3J = 4.9$ Hz, 4H, CH_2), 2.70 (dt, $^3J_{H,F} = 28.4$ Hz, $^3J = 4.9$ Hz, 2H, N-CH_2CH_2F), 2.48 (t, $^3J = 4.9$ Hz, 4H, CH_2), 1.46 ppm (s, 9H, CH_3); ^{13}C NMR (75.5 MHz, $CDCl_3$): $\delta = 154.68$, 81.85 ($|^1J_{C,F}| = 168.3$ Hz), 79.61, 58.23 ($|^2J_{C,F}| = 20.2$ Hz), 53.27, 48.90, 28.40 ppm; ^{19}F NMR (282 MHz, $CDCl_3$): $\delta = -218.25$ ppm; HRMS-ESI: *m/z* $[M+Na]^+$ calcd for $C_{11}H_{21}FN_2O_2Na$: 255.1479, found: 255.1455; Anal. calcd for $C_{11}H_{21}FN_2O_2$: C 56.87, H 9.11, N 12.06, found: C 57.09, H 9.32, N 12.30. *TFA salt*: yield = 46%, colorless solid; mp: 112–113 °C; ^{1}H NMR (300 MHz, $CDCl_3$): $\delta = 9.28$ (br s, 2H, NH_2^+), 4.72 (d, $^2J_{H,F} = 47.7$ Hz, 2H, N-CH_2CH_2F), 3.31–3.16 ppm (m, 10H, CH_2); ^{13}C NMR (75.5 MHz, $CDCl_3$): $\delta = 79.50$ ($|^1J_{C,F}| = 165.9$ Hz), 56.09 ($|^2J_{C,F}| = 19.1$ Hz), 48.69, 41.01 ppm; ^{19}F NMR (282 MHz, $CDCl_3$): $\delta = -218.46$; HRMS-ESI: *m/z* $[M]^+$ calcd for $C_6H_{14}FN_2$: 133.1136, found: 133.1146; Anal. calcd for $C_6H_{14}FN_2 \cdot 2$TFA: C 33.44, H 3.93, N 7.80, found: C 33.39, H 3.97, N 7.70.

4-(2-(2-(2-(2-Bromoethoxy)ethoxy)ethoxy)ethyl)piperazin-1-ium trifluoroacetate (9): *N-Boc-protected intermediate*: yield = 40%, light yellow oil; ^{1}H NMR (300 MHz, $CDCl_3$): $\delta = 3.83$–2.43 (m, 24H, CH_2), 1.46 ppm (s, 9H, CH_3); ^{13}C NMR (75.5 MHz, $CDCl_3$): $\delta = 154.70$, 79.53, 71.18, 70.65, 70.56, 70.51, 70.36, 68.81, 57.80, 53.33, 48.92, 30.31, 28.41 ppm; HRMS-ESI: *m/z* $[M+H]^+$ calcd for $C_{17}H_{34}BrN_2O_5$: 425.1645, found: 425.1649. *TFA salt*: yield = 47%, light yellow oil; ^{1}H NMR (300 MHz, $CDCl_3$): $\delta = 8.15$ (br s, 2H, NH_2^+), 3.80–2.99 ppm (m, 24H, CH_2); ^{13}C NMR (75.5 MHz, $CDCl_3$): $\delta = 71.21$, 71.06, 70.57, 70.39, 70.31, 66.56, 60.40, 56.96, 49.43, 30.48 ppm; HRMS-ESI: *m/z* $[M]^+$ calcd for $C_{12}H_{26}BrN_2O_3$: 325.1121, found: 325.1129.

4-(2-(2-(2-(2-Hydroxyethoxy)ethoxy)ethoxy)ethyl)piperazine (14): Compound **13** (10.0 g, 19.8 mmol; see Supporting Information) was stirred in MeOH (60 mL) containing concd HCl (10 mL) for 16 h. The solution was adjusted to pH 7.6 by adding solid $NaHCO_3$ (~10 g) and the resulting solution was diluted with water (200 mL). The precipitate (tritylmethylether) that formed upon addition of water was filtered off and the filtrate was evaporated to dryness. After the addition of CH_2Cl_2 (100 mL) the newly formed precipitate was removed by filtration. Concentration of the filtrate resulted in an orange oil; yield = 2.89 g (11.0 mmol, 56%); ^{1}H NMR (300 MHz, $CDCl_3$): $\delta = 3.78$–2.43 ppm (m, 24H, CH_2); ^{13}C NMR (75.5 MHz, $CDCl_3$): $\delta = 72.83$, 70.59, 70.51, 70.25, 70.21, 68.48, 61.49, 58.38, 54.73, 45.80 ppm; MS (MALDI-TOF): *m/z* 263 $[M+H]^+$; Anal. calcd for $C_{12}H_{26}N_2O_4$: C 54.94, H 9.99, N 10.68, found: C 52.62, H 9.86, N 10.35.

4-(2-(2-(2-(2-Fluoroethoxy)ethoxy)ethoxy)ethyl)piperazine (18): A solution of **17** (2.75 g, 10.0 mmol; see Supporting Information) and Cs_2CO_3 (4.88 g, 15.0 mmol) in abs DMF (60 mL) was treated with piperazine (**3**) (1.72 g, 20.0 mmol) and heated at 100 °C for 2 d. The solvent was then evaporated and the residue was taken up in EtOAc (120 mL). The precipitate was filtered off and the solvent was removed to give an orange oil, which was used in the next

step without further purification. The product contained traces of the dialkylated by-product (as seen by MS); yield = 2.48 g (9.38 mmol, 94%); ^{1}H NMR (300 MHz, $CDCl_3$): δ = 4.55 (dt, $^2J_{H,F}$ = 47.6 Hz, ^3J = 8.5 Hz, 2H, O-CH_2CH_2F), 3.81–2.45 ppm (m, 22H, CH_2); ^{13}C NMR (75.5 MHz, $CDCl_3$): δ = 83.11 ($|^1J_{C,F}|$ = 166.0 Hz), 70.84, 70.66, 70.56, 70.29, 69.70 ($|^2J_{C,F}|$ = 20.3 Hz), 68.88, 58.47, 55.08, 46.78 ppm; ^{19}F NMR (282 MHz, $CDCl_3$): δ = −221.55; MS (MALDI-TOF): *m/z* 265 $[M+H]^+$.

4-(3,6,9,12-Tetraoxapentadec-14-ynyl)piperazin-1-ium 2,2,2-trifluoroacetate (21): *N-Boc-protected intermediate*: yield = 70%, yellow oil; ^{1}H NMR (300 MHz, $CDCl_3$): δ = 4.20 (d, 2H, ^4J = 2.5 Hz, $CH_2C\equiv CH$), 3.70–2.44 (m, 25H, CH_2, CH), 1.46 ppm (s, 9H, CH_3); ^{13}C NMR (75.5 MHz, $CDCl_3$): δ = 154.70, 79.64, 79.55, 74.57, 70.62, 70.59, 70.57, 70.41, 70.38, 69.08, 68.84, 58.39, 57.82, 53.36, 49.03, 28.42 ppm; HRMS-ESI: *m/z* $[M+Na]^+$ calcd for $C_{20}H_{36}N_2O_6Na$: 423.2655, found: 423.2466; Anal. calcd for $C_{20}H_{36}N_2O_6$: C 59.98, H 9.06, N 6.99, found: C 59.06, H 9.07, N 7.02. *TFA salt*: yield = 86%, light yellow oil; ^{1}H NMR (300 MHz, $CDCl_3$): δ = 4.17 (d, 2H, ^4J = 2.4 Hz, $CH_2C\equiv CH$), 3.82–3.34 (m, 24H, CH_2, CH), 2.52 ppm (t, ^4J = 2.4 Hz, 1H, CH); ^{13}C NMR (75.5 MHz, $CDCl_3$): δ = 79.37, 75.04, 70.26, 70.24, 70.20, 70.00, 69.95, 69.85, 69.83, 58.20, 56.56, 51.90, 48.86 ppm; HRMS-ESI: *m/z* $[M]^+$ calcd for $C_{15}H_{29}N_2O_4$: 301.2122, found 301.2134; Anal. calcd for $C_{15}H_{29}N_2O_4\cdot$3TFA: C 39.38, H 4.56, N 4.37, found: C 39.47, H 5.04, N 4.58.

General procedure for the preparation of pyrimidine-2,4,6-triones 24 and 25–32: Compounds **24** and **25–32** were prepared according to the previously described procedures.[26,29]

5-(4-Phenoxyphenyl)-5-piperazinyl-pyrimidine-2,4,6-trione (25): Piperazine (**3**) was used to prepare this compound. For work up, the reaction mixture was taken up in EtOAc and water was added. The colorless precipitate was collected by suction; yield = 43%, colorless solid; mp: 275–277 °C (decomp); ^{1}H NMR (300 MHz, [D$_6$]DMSO): δ = 7.45–6.93 (m, 9H, H_{Aryl}), 2.68–2.19 ppm (m, 8H, CH_2); ^{13}C NMR (75.5 MHz, [D$_6$]DMSO): δ = 170.52, 157.10, 155.89, 150.30, 130.12, 129.81, 123.92, 119.87, 119.15, 117.93, 74.18, 48.69, 46.03 ppm; HRMS-ESI: *m/z* $[M+H]^+$ calcd for $C_{20}H_{21}N_4O_4$: 381.1563, found 381.1559; Anal. calcd for $C_{20}H_{20}N_4O_4\cdot0.5H_2O$: C 61.69, H 5.43, N 14.38, found: C 61.74, H 5.12, N 14.29.

5-[4-(2-Fluoroethyl)piperazin-1-yl]-5-(4-phenoxyphenyl)pyrimidine-2,4,6-trione (26): Compound **6** was used to prepare this compound. For work up, the reaction mixture was diluted with EtOAc and aqueous citric acid (0.1 mmol mL^{-1}) was added. The aqueous phase was extracted with EtOAc (2×) and the combined organic phases were washed with water, dried (Na_2SO_4), filtered and concentrated. The residue was purified by silica gel column chromatography (EtOAc/MeOH, 19:1) and the concentrated eluent was subsequently stirred in diisopropylether/acetone (99:1 *v/v*) to give pure **26**; yield = 45%; mp: 222–224 °C (decomp); ^{1}H NMR (300 MHz, [D$_6$]DMSO): δ = 11.46 (br s, 2H), 7.37–6.93 (m, 9H, H_{Aryl}), 4.43 (dt, $^2J_{H,F}$ = 48.0 Hz, $^3J_{H,H}$ = 9.6 Hz, 2H, N-CH_2CH_2F), 2.59–2.38 ppm (m, 10H, CH_2); ^{13}C NMR (75.5 MHz, [D$_6$]DMSO): δ = 169.92, 157.33, 155.74, 149.35, 130.13, 129.62, 129.56, 124.01, 119.23, 118.02, 81.65 ($|^1J_{C,F}|$ = 164.8 Hz), 73.87, 57.39 ($|^2J_{C,F}|$ = 19.7 Hz), 53.46, 47.23 ppm; HRMS-ESI: *m/z* $[M+H]^+$ calcd for $C_{22}H_{24}FN_4O_4$: 427.1776, found: 427.1779. The purity of **26** was determined by analytical HPLC to be > 97%, t_R = 20.64 ± 0.08 min (n = 3).

5-[4-(2-(2-(2-(2-Bromoethoxy)ethoxy)ethoxy)ethyl)piperazin-1-yl]-5-(4-phenoxyphenyl)pyrimidine-2,4,6-trione (27): Compound **9** was used to prepare this compound. For work up, water was added to the reaction mixture, which was subsequently extracted with EtOAc (3×). The combined extracts were washed with brine (1×), dried (Na_2SO_4), filtered and concentrated to give an orange oily residue. The residue was purified by silica gel column chromatography (EtOAc/MeOH, 19:1) to give pure **27**; yield = 36%; mp: 150 °C; ^{1}H NMR (300 MHz, [D$_6$]DMSO): δ = 11.59 (br s, 2H), 7.44–6.91 (m, 9H, H_{Aryl}), 3.68–2.32 ppm (m, 24H, CH_2); ^{13}C NMR (75.5 MHz, [D$_6$]DMSO): δ = 169.22, 157.22, 155.74, 149.36, 130.13, 129.62, 129.56, 124.00, 119.22, 118.00, 73.86, 70.30, 69.70, 69.57, 69.52, 68.22, 68.10, 57.05, 53.65, 47.23, 30.71 ppm; HRMS-ESI: *m/z* $[M+H]^+$ calcd for $C_{28}H_{35}BrN_4O_7$: 619.1764, found: 619.1762; Anal. calcd for $C_{28}H_{35}BrN_4O_7$: C 54.29, H 5.69, N 9.04, found: C 55.59, H 5.78, N 8.99.

5-[4-(2-(2-(2-(2-Hydroxyethoxy)ethoxy)ethoxy)ethyl)piperazin-1-yl]-5-(4-phenoxyphenyl)pyrimidine-2,4,6-trione (30): Compound **14** was used to prepare this compound. For work up, the solvent was evaporated and the residue purified by silica gel column chromatography (EtOAc/MeOH, 2:1) to give a highly viscous oil; yield = 55%; ^{1}H NMR (300 MHz, [D$_6$]DMSO): δ = 11.53 (br s, 2H), 7.38–6.93 (m, 9H, H_{Aryl}), 3.51–2.22 ppm (m, 24H, CH_2); ^{13}C NMR (75.5 MHz, [D$_6$]DMSO): δ = 169.98, 157.29, 155.75, 149.46, 130.52, 130.13, 129.63, 123.99, 119.21, 118.00, 73.84, 72.27, 69.74, 69.69, 69.57, 68.11, 60.12, 57.08, 53.67, 47.25, 29.46 ppm; HRMS-ESI: *m/z* $[M+H]^+$ calcd for $C_{28}H_{37}N_4O_8$: 557.2606, found: 557.2599. The purity of **30** was determined by analytical HPLC to be 95%, t_R = 20.93 ± 0.73 min (n = 5).

5-[4-(2-(2-(2-(2-Fluoroethoxy)ethoxy)ethoxy)ethyl)piperazin-1-yl]-5-(4-phenoxyphenyl)pyrimidine-2,4,6-trione (31): Compound **18** was used to prepare this compound. For work up, the solvent was evaporated and the residue purified by silica gel column chromatography (EtOAc/MeOH, 2:1) to give a highly viscous oil; yield = 32%; ^{1}H NMR (300 MHz, [D$_6$]DMSO): δ = 11.53 (br s, 2H), 7.36–6.91 (m, 9H, H_{Aryl}), 4.52 (d, $^2J_{H,F}$ = 48.5 Hz, 2H, O-CH_2CH_2F), 3.63–2.19 ppm (m, 22H, CH_2); ^{13}C NMR (75.5 MHz, [D$_6$]DMSO): δ = 169.86, 157.39, 155.65, 149.36, 130.15, 129.54, 126.94, 124.05, 119.21, 118.04, 83.00 ($|^1J_{C,F}|$ = 165.4 Hz), 73.82, 72.27, 70.15, 69.73, 69.64 ($|^2J_{C,F}|$ = 21.9 Hz), 69.46, 56.63, 53.36, 46.66, 30.11 ppm; HRMS-ESI: *m/z* $[M+H]^+$ calcd for $C_{28}H_{36}FN_4O_7$: 559.2563, found: 559.2557. The purity of **31** was determined by analytical HPLC to be 91%, t_R = 22.48 ± 0.07 min (n = 3).

5-[4-(3,6,9,12-Tetraoxapentadec-14-ynyl)piperazin-1-yl]-5-(4-phenoxyphenyl)pyrimidine-2,4,6-trione (32): Compound **21** was used as the piperazine component to prepare this compound. For work up, water was added to the reaction mixture, which was subsequently extracted with EtOAc (3×). The combined extracts were washed with brine (1×), dried (Mg_2SO_4) and filtered. The solvent was removed in vacuo and the residue purified by silica gel column chromatography (EtOAc/MeOH, 19:1) to give pure **32**; yield = 78%; mp: 155–157 °C; ^{1}H NMR (400 MHz, [D$_6$]DMSO): δ = 1.61 (br s, 2H), 7.42–6.99 (m, 9H, H_{Aryl}), 4.11 (s, 2H, CH_2-C≡CH), 3.53–2.48 (m, 25H, CH, CH_2); ^{13}C NMR (100 MHz, [D$_6$]DMSO): δ = 169.90, 157.33, 155.78, 149.35, 130.12, 129.64, 126.75, 124.00, 119.22, 118.02, 80.29, 77.02, 73.89, 69.97, 69.72, 69.69, 69.59, 69.45, 68.47, 68.11, 57.44, 57.07, 53.66, 47.25 ppm; HRMS-ESI: *m/z* $[M+H]^+$ calcd for $C_{31}H_{39}N_4O_8$: 595.2562, found: 595.2759; Anal. calcd for $C_{31}H_{38}N_4O_8$: C 62.61, H 6.44, N 9.42, found: C 62.33, H 6.40, N 9.29.

General procedure for the preparation of triazoles 36–38: Alkyne **32** (100 mg, 168 μmol) was dissolved in a mixture of *t*BuOH (6 mL) and H_2O (1.5 mL) under heating. The solution was cooled to RT and mesylate **33** (50 mg, 168 μmol), tosylate **34** (90 mg, 168 μmol), or fluoro compound **35** (37 mg, 168 μmol), $CuSO_4\cdot5H_2O$ (16.8 mg, 67.2 μmol, 40 mol% in case of **36** and **38** or 12.6 mg,

50.4 μmol, 30 mol% in case of **37**, respectively) as well as sodium ascorbate (26.6 mg, 13.4 μmol, 80 mol% in case of **36** and **38** or 13.3 mg, 67.2 μmol, 40 mol%, in case of **37**, respectively) were added in succession. After stirring at RT overnight, the solvents were removed and the residue purified by silica gel column chromatography (**36**: EtOAc/MeOH (4:1); **37**: EtOAc/MeOH (9:1) → EtOAc/MeOH (4:1); **38**: EtOAc/MeOH (1:1)). All eluted product fractions still contained 16–50% by-product (see below). Further purification was performed by preparative HPLC. The appropriate fractions (**36**: $t_R = 10.50$ min; **37**: $t_R = 10.48 \pm 0.03$ min ($n = 2$); **38**: $t_R = 10.38 \pm 0.08$ min ($n = 2$)) were collected and evaporated to give the pure (>95%, see below) triazoles **36**–**38** as colorless oils. The by-product (yields not determined), which could not be separated from the main products **36**–**38** by silica gel column chromatography turned out to be hydroxy compound **30**, as determined by analytical HPLC by co-injection with a sample of **30.** t_R(**30**) = 21.49 ± 0.12 min ($n = 4$), t_R(**36**) = 23.67 ± 0.02 min ($n = 2$), t_R(**37**) = 27.37 ± 0.07 min ($n = 5$), t_R(**38**) = 22.95 ± 0.04 min ($n = 2$); HRMS-ESI: *m/z* $[M+H]^+$ calcd for $C_{28}H_{37}N_4O_8$: 557.2606, found: 557.2599 (see above for **30**).

2-(2-(2-(2-(4-(13-(4-(2,4,6-Trioxo-5-(4-phenoxyphenyl)-hexa-hydropyrimidin-5-yl)piperazin-1-yl)-2,5,8,11-tetraoxatridecyl)-1*H*-1,2,3-triazol-1-yl)ethoxy)ethoxy)ethoxy)ethyl-methane-sufonate (36): yield = 29 mg (32 μmol, 19%); ^{1}H NMR (300 MHz, $CDCl_3$): δ = 7.74 (s, 1H, $CH_{Triazole}$), 7.50–6.94 (m, 9H, H_{Aryl}), 4.61 (s, 2H, $OCH_{2\ Triazole}$), 3.87–3.63 (m, 30H, CH_2), 3.04 (s, 3H, CH_3), 2.81–2.65 ppm (m, 10H, CH_2); ^{13}C NMR (75.5 MHz, $CDCl_3$): δ = 169.64, 158.09, 156.35, 149.59, 144.75, 130.03, 129.85, 128.89, 123.96, 123.85, 119.46, 118.19, 85.49, 70.62, 70.60, 70.52, 70.51, 70.46, 70.44, 70.40, 70.32, 70.21, 70.06, 69.53, 69.43, 69.01, 64.21, 53.50, 53.46, 50.21, 47.05, 37.65 ppm; HRMS-ESI: *m/z* $[M+H]^+$ calcd for $C_{40}H_{58}N_7O_{14}$: 892.3757, found: 892.3705. The purity was >95% as determined by analytical HPLC, t_R = 23.65 min.

2-(2-(2-(2-(4-(13-(4-(2,4,6-Trioxo-5-(4-phenoxyphenyl)hexa-hydropyrimidin-5-yl)piperazin-1-yl)-2,5,8,11-tetraoxatridecyl)-1*H*-1,2,3-triazol-1-yl)ethoxy)ethoxy)ethoxy)ethyl-4-methyl-benzene-sulfonate (37): yield = 34 mg (36 μmol, 30%); ^{1}H NMR (300 MHz, $CDCl_3$): δ = 7.80–6.94 (m, 14H, H_{Aryl}, $H_{Triazole}$), 4.68 (s, 2H, $OCH_{2\ Triazole}$), 4.12–3.60 (m, 30H, CH_2), 2.82–2.65 (m, 10H, CH_2) 2.43 ppm (s, 3H, CH_3); ^{13}C NMR (75.5 MHz, $CDCl_3$): δ = 169.50, 158.14, 156.36, 149.35, 144.88, 144.72, 132.93, 130.07, 129.88, 129.87, 124.05, 123.89, 123.88, 119.52, 119.50, 118.22, 86.34, 70.72, 70.60, 70.47, 70.43, 70.39, 70.33, 70.28, 70.25, 70.19, 70.14, 69.47, 69.40, 69.26, 68.68, 67.71, 57.43, 53.48, 50.21, 47.09, 21.66 ppm; HRMS-ESI: *m/z* $[M+H]^+$ calcd for $C_{46}H_{62}N_7O_{14}S$: 968.4070, found 968.3837. The purity was >95% as determined by semipreparative HPLC, t_R = 14.30 min.

5-(4-(1-(1-(2-(2-(2-(2-Fluoroethoxy)ethoxy)ethoxy)ethyl)-1*H*-1,2,3-triazol-4-yl-)-2,5,8,11-tetraoxa-tridecan-13-yl)piperazin-1-yl)-5-(4-phenoxyphenyl)pyrimidine-2,4,6-trione (38): yield = 44 mg (54 μmol, 32%); ^{1}H NMR (300 MHz, $CDCl_3$): δ = 7.75 (s, 1H, $CH_{Triazole}$), 7.37–6.94 (m, 9H, H_{Aryl}), 4.54 (dt, $^2J_{H,F}$ = 47.7 Hz, 2H, O-CH_2CH_2F), 4.51 (s, 2H, $OCH_{2Triazole}$), 3.87–2.68 ppm (m, 38H, CH_2); ^{13}C NMR (75.5 MHz, $CDCl_3$): δ = 169.62, 158.10, 156.39, 149.53, 144.77, 129.87, 128.94, 124.00, 123.85, 119.48, 118.21, 88.16, 83.15 ($|^1J_{C,F}|$ = 169.6 Hz), 70.63 ($|^2J_{C,F}|$ = 20.2 Hz), 70.61, 70.54, 70.50, 70.48, 70.45, 70.42, 70.38, 70.32, 70.31, 70.27, 69.51, 69.43, 64.27, 57.35, 53.47, 50.24, 42.11 ppm; ^{19}F NMR (282 MHz, $CDCl_3$): δ = −222.67 ppm; HRMS-ESI: *m/z* $[M+H]^+$ calcd for $C_{39}H_{55}FN_7O_{11}$: 816.3938, found: 816.3898. The purity was >95% as determined by semipreparative HPLC, t_R = 12.17 ± 0.01 min ($n = 2$).

Radiochemistry

General methods: Radiofluorinations were carried out on a modified PET tracer radiosynthesizer (TRACERLab Fx_{FDG}, GE Healthcare, http://www.gehealthcare.com/eude/fun_img/products/radiopharmacy/products/tracercenter_tracerlabs.html). The recorded data were processed by the TRACERLab Fx software (GE Healthcare). Separation and purification of the radiosynthesized compounds were—unless specified otherwise—performed by a gradient radio-HPLC chromatography system (HPLC A) using a Knauer K-500 and a Latek P 402 pump, a Knauer K-2000 UV-detector (λ = 254 nm) a Crismatec NaI(Tl) Scintibloc 51 SP51 γ-detector and a RP-HPLC Nucleosil column 100–10 C-18 (250 mm × 8 mm), a corresponding precolumn (20 mm × 4.0 mm). Sample injection was carried out using a Rheodyne injector block (type 7125 including a 200 μL loop). The recorded data were processed by the NINA version 4.9 software (GE Medical Systems). The radiochemical purities and the specific activities were determined using a radio-HPLC system (HPLC B) composed of a Syknm S1021 pump, a Knauer K-2501 UV-detector (λ = 254 nm), a Crismatec NaI(Tl) Scintibloc 51 SP51 γ-detector, a RP-HPLC Nucleosil 100–3 C-18 column (200 mm × 3 mm), a VICI injector block (type C1 including a 20 μL loop) and the GINA Star version 4.07 radiochromatography software (Raytest Isotopenmeßgeräte GmbH). Radio-TLC plates were analyzed using a miniGITA TLC-Scanner (Raytest Isotopenmeßgeräte GmbH).

Production of [^{18}F]fluoride and synthesis of [^{18}F]K(K_{222})F: No-carrier-added aqueous [^{18}F]fluoride was produced on a RDS 111e cyclotron (CTI-Siemens) by irradiation of a 1.2 mL water target using 10 MeV proton beams on 97.0% enriched ^{18}O-water by the ^{18}O(p,n)^{18}F nuclear reaction. Typical batches of [^{18}F]fluoride ions were 8.1 GBq (in the case of the generation of [^{18}F]**26**) and 2.7 GBq (in the case of radiofluorination of tosylate **37**) at the end of radionuclide production for currents of 32 μA and irradiation times of 10 or 4 min, respectively. To recover the ^{18}O-water, the batch of aqueous [^{18}F]fluoride was passed through an anion exchange resin (Sep-Pak Light Waters Accell Plus QMA cartridge, preconditioned with 5 mL 1 M K_2CO_3 and 10 mL water). [^{18}F]Fluoride was eluted from the resin with a mixture of 40 μL 1 M K_2CO_3, 200 μL water for injection and 800 μL DNA-grade CH_3CN containing 18 mg K_{222}. Subsequently, the aqueous [^{18}F]K(K_{222})F solution was carefully evaporated to dryness in vacuo.

5-[4-(2-[^{18}F]Fluoroethyl)piperazin-1-yl]-5-(4-phenoxyphenyl)pyrimidine-2,4,6-trione ([^{18}F]26): Ethylene glycol di-*p*-tosylate (5.0 mg, 13.5 μmol) in DNA-grade CH_3CN (1 mL) was added to the carefully dried [^{18}F]K(K_{222})F residue (see above) and the mixture was heated at 84 °C for 4 min. The mixture was cooled to 40 °C, diluted with water (10 mL) and passed through a Waters Sep-Pak Light C18 cartridge. The cartridge was washed with additional water (10 mL) and dried under a flow of He for 10–20 min, followed by elution of 1-[^{18}F]fluoro-2-tosyloxyethane ([^{18}F]**5**) with hot DMSO (400 μL, heated to 120 °C prior to elution) into a 5 mL flask containing precursor **25** (4.0 mg, 10.5 μmol) and DMSO (100 μL). [^{18}F]**5** was obtained in a radiochemical yield of 53.3 ± 2.3% (decay-corrected, n = 6). The following steps were performed outside the synthesizer.

The reaction mixture was stirred at 120 °C for 15 min, diluted with water (400 μL) and applied to the HLPC column (see general methods section above). HPLC A; conditions: eluent A: CH_3CN/H_2O/TFA (950:50:1), eluent B: CH_3CN/H_2O/TFA (50:950:1); gradient: 75% eluent B, after elution of the product 30% eluent B for 20 min at a flow rate of 4.0 mL min^{-1}, λ = 254 nm. The appropriate fraction ([^{18}F]**26**: t_R = 27.1 min) was collected, evaporated to dryness in vacuo and redissolved in 1 mL H_2O/EtOH (9:1). [^{18}F]**26** was synthe-

sized with radiochemical yields of 21.3±4.0% (decay-corrected, $n=6$) starting from [^{18}F]**5**. The overall radiochemical yields of this two-step radiosynthesis were 11.3±2.2% (decay-corrected, based on cyclotron-derived [^{18}F]fluoride ions). The radiochemical purities were 98.5±1.5% after 142±12 min from the end of radionuclide production. The determined specific radioactivity (A_s) was 23± 10 GBq μmol^{-1} at the end of radiosynthesis ($n=6$). The A_s of product [^{18}F]**26** was estimated by comparing the peak area of purified [^{18}F]**26** in the UV channel ($t_R=8.4$ min, HPLC B) with a standard curve of known concentrations of reference compound **26** measured with the HPLC B system (flow rate: 0.3 mL min^{-1}; eluent: CH_3CN/H_2O/TFA (400:600:1)). The chemical identity of [^{18}F]**26** was proven by two different chromatographical methods. 1) HPLC: Co-injection of [^{18}F]**26** and non-radioactive counterpart **26** resulted in co-elution on the HPLC A and B systems. 2) Radio-TLC: Both [^{18}F]**26** and non-radioactive counterpart **26** possessed the same R_f value ($R_f=0.69$ (EtOAc/MeOH, 4:1); silica gel UV_{254}).

Reaction of tosylate precursor 37 with [^{18}F]K(K_{222})F: Tosylate precursor **37** (4.2 mg, 4.34 μmol) and carefully dried [^{18}F]K(K_{222})F (see above) residue were heated at 84 °C in DNA-grade CH_3CN (1 mL) for 20 min. The mixture was cooled to 40 °C, diluted with water for injection (10 mL) and passed through a Waters Sep-Pak Light C18 cartridge. The cartridge was washed with additional water for injection (10 mL) and eluted with hot DMF (2.0 mL, heated to 120 °C prior to elution). The eluent was evaporated to dryness, diluted with CH_3CN/water (1:1; 1.0 mL) for injection, vortexed and purified *by* semipreparative gradient HPLC (see the general methods under the Chemistry section). By collecting and evaporating of the appropriate fractions, only a small amount of radiofluorinated product [^{18}F]**38** ($t_R=12.35$ min) was discovered. Interestingly, a non-radioactive product fraction ($t_R=12.43$ min) was isolated. The radiofluorinated product was presumably [^{18}F]**38**. As the radiochemical yield was ≤1% the identity of this product with its unlabeled analogue **38** was not verified. The tosylate precursor **37** ($t_R=14.30$ min) was not recovered in the UV channel of the radio-HPLC system. The non-radioactive product was examined by MS: HRMS-ESI: m/z $[M+H]^+$ calcd for $C_{39}H_{54}N_7O_{11}$: 796.3876, found: 796.3863. The identity of this product is delineated in the Discussion section.

Measurement of log *D* value: Determination of the log *D* value of [^{18}F]**26** was performed in 1-octanol and 0.02 M phosphate buffer at pH 7.4 as described previously.[45,46] The liquid layers were counted in an automated gamma counter (Wallac Wizard 3″, Perkin–Elmer Life Sciences, Boston, USA), and the measured counts were back corrected for decay. The measurement was repeated four times. The log *D* value was determined by calculating the 1-octanol-to-buffer ratios:

$$\log D = \log\left(\frac{\text{cpm mL}^{-1}\ \text{octanol}}{\text{cpm mL}^{-1}\ \text{buffer}}\right)$$

Biology

Enzyme inhibition assays

The synthetic fluorogenic substrate (7-methoxycoumarin-4-yl)acetyl-pro-Leu-Gly-Leu-(3-(2,4-dinitrophenyl)-L-2,3-diamino-propionyl)-Ala-Arg-NH_2 (R&D Systems, Minneapolis, USA) was used to assay activated MMP-2, MMP-8, MMP-9 and MMP-13 as described previously.[30] The inhibition of human active MMPs by the barbituric acid derivatives **25**–**32** and **38** were assayed by preincubating MMP-1, MMP-2, MMP-3, MMP-8, MMP-9, MMP-13 or MMP-14 (each at 2 nM) and test compounds at varying concentrations (10 pM–1 mM) in Tris·HCl (50 mM), pH 7.5, containing NaCl (0.2 M), $CaCl_2$ (5 mM), $ZnSO_4$ (20 μM) and 0.05% Brij 35 at 37 °C for 30 min. An aliquot of substrate (10 μL of a 50 μM solution) was then added to the preincubated MMP/inhibitor mixture (90 μL), and the fluorescence was determined at 37 °C by following product release over time. The fluorescence changes were monitored using a Fusion Universal Microplate Analyzer (Packard Bioscience, Massachusetts, USA) with excitation and emission wavelengths of 330 and 390 nm, respectively. Reaction rates were measured from the initial 10 min of the reaction profile where product release was linear with time and plotted as a function of inhibitor concentration. From the resulting inhibition curves, the IC_{50} values for each inhibitor were calculated by nonlinear regression analysis, performed using the Grace 5.1.8 software (Linux).

Animal studies

Studies were carried out according to protocols approved by the local ethics committee and were performed in accordance with institutional guidelines for health and care of experimental animals.

*Biodistribution of [^{18}F]**26***: Adult C57/BL6 mice (male, ~29 g) were anaesthetized by isoflurane/O_2 and one lateral tail vein was cannulated using a 27 G needle connected to 15 cm polyethylene catheter tubing (o.d.=1.09 mm, i.d.=0.38 mm). [^{18}F]**26** (315 MBq kg^{-1}) was injected as a bolus (200 μL) via the tail vein, and subsequent PET scanning was performed. To outline the position of the heart, [^{18}F]FDG (4 MBq in 200 μL per mouse) was injected via the tail vein 5 min after completion of the scan with [^{18}F]**26**, and data were acquired for a further 30 min.

Small-animal PET scanning: PET experiments were carried out using a sub-millimeter high-resolution (0.7 mm full width at half maximum) dedicated small-animal scanner (32 module quadHIDAC, Oxford Positron Systems Ltd., Oxford, UK), which uses wire-chamber detectors and offers uniform spatial resolution (<1 mm) over a large cylindrical field (165 mm diameter, 280 mm axial length).[47–49] List-mode data were acquired for 120 min and reconstructed into dynamic time frames using an iterative reconstruction algorithm.[50] PET images were analyzed using in-house software algorithms in MATLAB (The MathWorks Company) and C programming languages.[48,51] For in vivo biodistribution measurements of [^{18}F]**26** regions-of-interest (ROIs) were drawn over selected tissues/organs in five coronal planes. For precise placement of ROIs, representing arterial blood pool image data was resliced according to heart coordinates and ROIs were defined on five short axis planes of the left ventricle.

Glossary

EG, ethylene glycol; EM, exact mass; ESI, electron spray ionization; [^{18}F]FDG, 2-deoxy-2-[^{18}F]fluoro-D-glucose; K_{222}, Kryptofix 2.2.2; MMP, matrix metalloproteinase; MMPI, matrix metalloproteinase inhibitor; NHS, *N*-hydroxysuccinimidyl; NIRF, near-infrared fluorescence; NOE, Nuclear Overhauser Effect; PEG, polyethylene glycol; PET, positron emission tomography; p.i., post injection; ROI, region of interest; SD, standard deviation; SPECT, single photon emission computed tomography.

Acknowledgements

This work was supported by grants from the Deutsche Forschungsgemeinschaft (DFG; Münster, Germany; Projects SFB

656A2, B1, C6 and Z5) and the Interdisciplinary Center of Clinical Research (IZKF; Münster, Germany; Project Schä2/020/09 & core unit SmAP). We thank Sandra Schröer for her excellent technical assistance, K. Bergander and H. Luftmann (Department of Organic Chemistry, WWU Münster) for performing NMR spectroscopy and mass spectrometry, respectively, and S. Fatum for further technical assistance.

Keywords: fluorinated ligands · inhibitors · metalloenzymes · positron emission tomography · pyrimidine-2,4,6-triones · radiochemistry

[1] A. R. Folgueras, A. M. Pendas, L. M. Sanchez, C. López-Otín, *Int. J. Dev. Biol.* **2004**, *48*, 411 – 424.
[2] C. M. Overall, C. López-Otín, *Nat. Rev. Cancer* **2002**, *2*, 657 – 672.
[3] M. H. Tayebjee, G. Y. Lip, R. J. MacFadyen, *Curr. Med. Chem.* **2005**, *12*, 917 – 925.
[4] I. Stamenkovic, *J. Pathol.* **2003**, *200*, 448 – 464.
[5] P. Vihinen, R. Ala-aho, V. M. Kahari, *Curr. Cancer Drug Targets* **2005**, *5*, 203 – 220.
[6] M. Egeblad, Z. Werb, *Nat. Rev. Cancer* **2002**, *2*, 161 – 174.
[7] S. Heeneman, J. P. Cleutjens, B. C. Faber, E. E. Creemers, R.-J. van Suylen, E. Lutgens, K. B. Cleutjens, M. J. Daemen, *J. Pathol.* **2003**, *200*, 516 – 525.
[8] Z. S. Galis, J. J. Khatri, *Circ. Res.* **2002**, *90*, 251 – 262.
[9] Z. S. Galis, *Circulation* **2004**, *110*, 244 – 246.
[10] A. C. Newby, *Physiol. Rev.* **2005**, *85*, 1 – 31.
[11] K. Kopka, H.-J. Breyholz, S. Wagner, M. P. Law, B. Riemann, S. Schröer, M. Trub, B. Guilbert, B. Levkau, O. Schober, M. Schäfers, *Nucl. Med. Biol.* **2004**, *31*, 257 – 267.
[12] M. Schäfers, B. Riemann, K. Kopka, H.-J. Breyholz, S. Wagner, K. P. Schäfers, M. P. Law, O. Schober, B. Levkau, *Circulation* **2004**, *109*, 2554 – 2559.
[13] H. Su, F. G. Spinale, L. W. Dobrucki, J. Song, J. Hua, S. Sweterlitsch, D. P. Dione, P. Cavaliere, C. Chow, B. N. Bourke, X. Y. Hu, M. Azure, P. Yalamanchili, R. Liu, E. H. Cheesman, S. Robinson, D. S. Edwards, A. J. Sinusas, *Circulation* **2005**, *112*, 3157 – 3167.
[14] J. Zhang, L. Nie, M. Razavian, M. Ahmed, L. W. Dobrucki, A. Asadi, D. S. Edwards, M. Azure, A. J. Sinusas, M. M. Sadeghi, *Circulation* **2008**, *118*, 1953 – 1960.
[15] S. Ohshima, A. Petrov, S. Fujimoto, J Zhou, M. Azure, D. S. Edwards, T. Murohara, N. Narula, S. Tsimikas, J. Narula, *J. Nucl. Med.* **2009**, *50*, 612 – 617.
[16] J. F. Fisher, S. Mobashery, *Cancer Metastasis Rev.* **2006**, *25*, 115 – 136.
[17] E. Nuti, T. Tuccinardi, A. Rossello, *Curr. Pharm. Des.* **2007**, *13*, 2087 – 2100.
[18] E. Breuer, J. Frant, R. Reich, *Expert Opin. Ther. Pat.* **2005**, *15*, 253 – 269.
[19] C. A. Corbitt, J. Lin, M. L. Lindsey, *Recent Pat. Anti-Cancer Drug Discovery* **2007**, *2*, 135 – 142.
[20] F. Grams, H. Brandstetter, S. D'Alo, D. Geppert, H. W. Krell, H. Leinert, V. Livi, E. Menta, A. Oliva, G. Zimmermann, *Biol. Chem.* **2001**, *382*, 1277 – 1285.
[21] H. Brandstetter, F. Grams, D. Glitz, A. Lang, R. Huber, W. Bode, H. W. Krell, R. A. Engh, *J. Biol. Chem.* **2001**, *276*, 17405 – 17412.
[22] L. H. Foley, R. Palermo, P. Dunten, *Bioorg. Med. Chem. Lett.* **2001**, *11*, 969 – 972.
[23] E. Maquoi, N. E. Sounni, L. Devy, F. Olivier, F. Frankenne, H. W. Krell, F. Grams, J. M. Foidart, A. Noël, *Clin. Cancer Res.* **2004**, *10*, 4038 – 4047.
[24] B. Fingleton, *Expert Opin. Ther. Targets* **2003**, *7*, 385 – 397.
[25] H.-J. Breyholz, M. Schäfers, S. Wagner, C. Höltke, A. Faust, H. Rabeneck, B. Levkau, O. Schober, K. Kopka, *J. Med. Chem.* **2005**, *48*, 3400 – 3409.
[26] A. Faust, B. Waschkau, J. Waldeck, C. Höltke, H. J. Breyholz, S. Wagner, K. Kopka, W. Heindel, M. Schäfers, C. Bremer, *Bioconjugate Chem.* **2008**, *19*, 1001 – 1008.
[27] a) H.-J. Breyholz, A. Faust, B. Waschkau, S. Wagner, C. Höltke, J. Waldeck, W. Brandau, C. Bremer, O. Schober, M. Schäfers, K. Kopka, *Q. J. Nucl. Med. Mol. Imaging* **2008**, *52*, *N. 1*, 23 – 25; b) H.-J. Breyholz, A. Faust, B. Waschkau, S. Wagner, C. Höltke, J. Waldeck, W. Brandau, C. Bremer, O. Schober, M. Schäfers, K. Kopka, *Eur. J. Nucl. Med. Mol. Imaging* **2008**, *35*, *Suppl. 2*, S316.
[28] C. Tahtaoui, I. Parrot, P. Klotz, F Guillier, J.-L. Galzi, M. Hibert, B. Ilien, *J. Med. Chem.* **2004**, *47*, 4300 – 4315.
[29] S. Hutchings, W. Liu, R. Radinov, *Heterocycles* **2006**, *67*, 763 – 768.
[30] W. Huang, Q. Meng, K. Suzuki, H. Nagase, K. Brew, *J. Biol. Chem.* **1997**, *272*, 22086 – 22091.
[31] U. Sirion, H. J. Kim, J. H. Lee, J. W. Seo, B. S. Lee, S. J. Lee, S. J. Oh, D. Y. Chi, *Tetrahedron Lett.* **2007**, *48*, 3953 – 3957.
[32] a) J. M. Harris, R. B. Chess, *Nat. Rev. Drug Discovery* **2003**, *2*, 214 – 221; b) J. M. Harris, N. E. Martin, M. Modi, *Clin. Pharmacokinet.* **2001**, *40*, 539 – 551; c) M. Hamidi, A. Azadi, P. Rafiei, *Drug Delivery* **2006**, *13*, 399 – 409.
[33] a) Z. Wu, Z. B. Li, K. Chen, W. Cai, L. He, F. T. Chin, F. Li, X. Chen, *J. Nucl. Med.* **2007**, *48*, 1536 – 1544; b) Z. Liu, S. Liu, F. Wang, S. Liu, X. Chen, *Eur. J. Nucl. Med. Mol. Imaging* **2009**, *36*, 1296 – 1307; c) Z. Liu, G. Niu, J. Shi, S. Liu, F. Wang, S. Liu, X. Chen, *Eur. J. Nucl. Med. Mol. Imaging* **2009**, *36*, 947 – 957; d) L. Wang, J. Shi, Y. S. Kim, S. Zhai, B. Jia, H. Zhao, Z. Liu, F. Wang, X. Chen, S. Liu, *Mol. Pharm.* **2009**, *6*, 231 – 245.
[34] Q. Wang, K. Graham, T. Schauer, T. Fietz, A. Mohammed, X. Liu, J. Hoffend, U. Haberkorn, M. Eisenhut, W. Mier, *Nucl. Med. Biol.* **2004**, *31*, 21 – 30.
[35] R. B. Pepinsky, W.-C. Lee, M. Cornebise, A. Gill, K. Wortham, L. L. Chen, D. R. Leone, K. Giza, B. M. Dolinski, S. Perper, C. Nickerson-Nutter, D. Lepage, A. Chakraborty, E. T. Whalley, R. C. Petter, S. P. Adams, R. R. Lobb, D. M. Scott, *J. Pharmacol. Exp. Ther.* **2004**, *312*, 742 – 750.
[36] W. Zhang, M. P. Kung, S. Oya, C. Hou, H. F. Kung, *Nucl. Med. Biol.* **2007**, *34*, 89 – 97.
[37] G. C. Tron, T. Pirali, R. A. Billington, P. L. Canonico, G. Sorba, A. Genazzani, *Med. Res. Rev.* **2008**, *28*, 278 – 308.
[38] Y. L. Angell, K. Burgess, *Chem. Soc. Rev.* **2007**, *36*, 1674 – 1689.
[39] A. D. Moorhouse, J. E. Moses, *ChemMedChem* **2008**, *3*, 715 – 723.
[40] C. D. Hein, X. M. Liu, D. Wang, *Pharm. Res.* **2008**, *25*, 2216 – 2230.
[41] W. S. Horne, M. K. Yadav, C. D. Stout, M. R. Ghadiri, *J. Am. Chem. Soc.* **2004**, *126*, 15366 – 15367.
[42] A. D. Moorhouse, A. M. Santos, M. Gunaratnam, M. Moore, S. Neidle, J. E. Moses, *J. Am. Chem. Soc.* **2006**, *128*, 15972 – 15973.
[43] C. Mamat, T. Ramenda, F. R. Wuest, *Mini-Rev. Org. Chem.* **2009**, *6*, 21 – 34.
[44] Z. B. Li, Z. Wu, K. Chen, F. T. Chin, X. Chen, *Bioconjugate Chem.* **2007**, *18*, 1987 – 1994.
[45] A. A. Wilson, S. Houle, *J. Labelled Compd. Radiopharm.* **1999**, *42*, 1277 – 1288.
[46] A. A. Wilson, L. Jin, A. Garcia, J. N. DaSilva, S. Houle, *Appl. Radiat. Isot.* **2001**, *54*, 203 – 208.
[47] A. P. Jeavons, R. A. Chandler, C. A. R. Dettmar, *IEEE Trans. Nucl. Sci.* **1999**, *46*, 468 – 473.
[48] K. P. Schäfers, A. J. Reader, M. Kriens, C. Knoess, O. Schober, M. Schäfers, *J. Nucl. Med.* **2005**, *46*, 996 – 1004.
[49] J. Missimer, Z. Madi, M. Honer, C. Keller, P. A. Schubiger, S.-M. Ametamey, *Phys. Med. Biol.* **2004**, *49*, 2069 – 2081.
[50] A. J. Reader, S. Ally, F. Bakatselos, R. Manavaki, R. J. Walledge, A. P. Jeavons, P. J. Julyan, Z. Sha, D. L. Hastings, J. Zweit, *IEEE Trans. Nucl. Sci.* **2002**, *49*, 693 – 699.
[51] S. Biedenstein, M. Schäfers, L. Stegger, T. Kuwert, O. Schober, *Eur. J. Nucl. Med.* **1999**, *26*, 201 – 207.

Received: January 13, 2010
Revised: March 5, 2010
Published online on April 1, 2010

